



Deposited via The University of Leeds.

White Rose Research Online URL for this paper:

<https://eprints.whiterose.ac.uk/id/eprint/129923/>

Version: Accepted Version

---

**Article:**

Harvie, AJ, Smith, CT, Ahumada-Lazo, R et al. (2018) Ultrafast Trap State-Mediated Electron Transfer for Quantum Dot Redox Sensing. *Journal of Physical Chemistry C*, 122 (18). pp. 10173-10180. ISSN: 1932-7447

<https://doi.org/10.1021/acs.jpcc.8b02551>

---

© 2018 American Chemical Society. This document is the Accepted Manuscript version of a Published Work that appeared in final form in *Journal of Physical Chemistry C*, copyright © American Chemical Society after peer review and technical editing by the publisher. To access the final edited and published work see <https://doi.org/10.1021/acs.jpcc.8b02551>. Uploaded in accordance with the publisher's self-archiving policy.

**Reuse**

Items deposited in White Rose Research Online are protected by copyright, with all rights reserved unless indicated otherwise. They may be downloaded and/or printed for private study, or other acts as permitted by national copyright laws. The publisher or other rights holders may allow further reproduction and re-use of the full text version. This is indicated by the licence information on the White Rose Research Online record for the item.

**Takedown**

If you consider content in White Rose Research Online to be in breach of UK law, please notify us by emailing [eprints@whiterose.ac.uk](mailto:eprints@whiterose.ac.uk) including the URL of the record and the reason for the withdrawal request.

## Ultrafast Trap-state Mediated Electron Transfer for Quantum Dot Redox Sensing

Andrew J. Harvie<sup>1</sup> Charles T. Smith<sup>2</sup>, Ruben Ahumada-Lazo<sup>2</sup>, Lars J. C. Jeuken<sup>3,4</sup>, Marco Califano<sup>5</sup>, Robin S. Bon<sup>4,6</sup>, Samantha J. O. Hardman<sup>7</sup>, David J. Binks<sup>2</sup>, Kevin Critchley<sup>1\*</sup>.

<sup>1</sup>School of Physics and Astronomy, <sup>3</sup>School of Biomedical Sciences, <sup>4</sup>Astbury Centre, <sup>5</sup>Pollard Institute, School of Electronic and Electrical Engineering, and <sup>6</sup>Leeds Institute of Cardiovascular and Metabolic Medicine, University of Leeds, Leeds, LS2 9JT. United Kingdom

<sup>2</sup>School of Physics and Astronomy and Photon Science Institute, <sup>7</sup> Manchester Institute of Biotechnology, The University of Manchester, Manchester, M13 9PL. United Kingdom

\*Email: [k.critchley@leeds.ac.uk](mailto:k.critchley@leeds.ac.uk)

### Abstract

Quantum dots (QDs) conjugated to electron acceptor ligands are useful as redox sensors in applications ranging from chemical detection to bioimaging. We aimed to improve effectiveness of these redox-sensing QD conjugates, which depends on the initial charge separation and on the competing mechanisms of recombination, including luminescence and electron transfer to the conjugated redox molecules. In this study, ultrafast laser measurements were used to study the excited state dynamics in CdTe/CdS core/shell QDs with quinone/quinol acceptor (Q2NS) ligands attached to the surface (up to 40 per QD). Detailed analysis, along with computational modelling of the system, showed multiple electron transfer pathways and identified an ultrafast electron transfer from a surface electron trap state to the quinone ligands (2-8 ps). We propose that this leads to high, redox-dependent, quenching efficiencies (98.7% with an average of 10 quinone/quinols on the surface). As only low populations of redox ligands are required, the colloidal properties of the QD are preserved, which allows for further functionalisation. These new insights into the excited state properties and ultra-fast charge transfer has important implications for fields exploring charge extraction from quantum dots, which range from bioimaging to solar energy technology.

## 1. Introduction

The unique size-dependent properties of quantum dots (QDs) have made them one of the most widely researched areas of nanotechnology. They have many applications including quantum cryptography,<sup>1</sup> photovoltaics,<sup>2</sup> display technologies,<sup>3</sup> bioimaging, and biosensing.<sup>4</sup> In the cases of biological (or chemical) sensing, QDs provide many advantages: they are more resistant to photobleaching than conventional fluorophores, their luminescence can be finely controlled via the size of the nanoparticles, and their colloidal properties and interactions with biology can be modified by surface functionalisation.<sup>5</sup>

Nanoscale redox sensors have found important applications in monitoring the redox potential within live cells, with particular interest in the differences between cells of different disease states; more oxidative potentials have been implicated in a variety of disease states including neurodegenerative conditions and cancer.<sup>6,7</sup> For instance, the Warburg effect, which characterises many cancers, triggers dysregulation of redox potential as a result of the heightened dependence on glycolysis for energy production.<sup>8,9</sup> There are a wide range of redox sensing strategies, from redox sensitive dyes such as 5-cyano-2, 3-ditoly tetrazolium chloride (CTC)<sup>10</sup> to functionalised nanoparticles. Nanoparticles used in redox sensing range from gold nanoparticles for surface-enhanced Raman sensing,<sup>6</sup> to QDs that allow fluorimetric measurement. Redox-based sensing is also useful for applications outside of the cell; redox-sensitive QDs have been applied for pH sensing,<sup>11</sup> detection of explosives,<sup>12</sup> as well as detection and investigation of biological analytes.<sup>4, 7, 12, 13</sup>

Redox, or pH sensitive QDs commonly operate on the principle of an interaction between the charge carriers within the QD and some conjugated redox-active ligand. This usually involves a charge, or energy, transfer event between the QD and the molecular adsorbate, which becomes more (or less) favourable depending on the redox state of the ligand.<sup>5, 14</sup> This transfer event then results in a quenching of the luminescence of the QD conjugate system. Ligands commonly used for this purpose include redox sensitive dyes, fluorophores, or electron acceptors such as quinone<sup>7, 11</sup> or nicotinamide adenine dinucleotide (NADH) derivatives.<sup>12</sup> Quinone-derived compounds are common due to their well-understood redox behaviour, synthetic simplicity, and relevance to biological systems.

Understanding the time dynamics of the charge transfer process between a QD and its conjugate enables strategies to be designed to enhance the efficiency of transfer and limit the impact of any competing processes. Charge extraction from QDs is already a widely studied field<sup>15</sup> since efficient transfer is often necessary for good device performance. For example, in photovoltaics, extraction is required before charges recombine either radiatively, with typical timescales of tens to hundreds of ns, or non-radiatively, where trapping or Auger recombination can occur in the first few ps after excitation.<sup>16</sup> While it is often straightforward to predict steady-state optical properties of QDs of a number of different materials given information about particle size and band gap, the excited state dynamics in QDs often vary greatly between QDs, therefore the topic of excited state dynamics in QDs and QD-conjugate systems is of broad discussion in the literature.<sup>17</sup>

For effective redox-sensitive QDs, a system must be designed which exhibits a switchable, luminescence-quenching charge or energy transfer process that is significantly faster than the timescale associated with radiative recombination. For sensors based on charge transfer, this can be achieved either by increasing the radiative recombination timescale, decreasing the charge transfer timescale (or by employing a combination of the two). CdTe/CdS core-shell QDs exhibit a type-II heterostructure which results in spatial separation of the electron and hole after excitation. The band alignment is such that a photoexcited electron will be confined to the CdS shell, with the resulting hole being confined to the core. Thinner CdS shells will result in a quasi-type-II alignment where the hole is

confined to the CdTe core, and the electron is delocalized across the whole QD. This charge separation greatly increases the recombination lifetime vs the core-only QDs, even for thin shells.<sup>18-20</sup> Another advantage of the charge separation is the expected increase in charge extraction efficiency due to the location of the electron on the CdS surface.<sup>20</sup>

In this article, we discuss a new redox-sensing QD-acceptor conjugate system comprised of CdTe/CdS QDs conjugated with a number of the quinone molecules (Q2NS). Q2NS is an electron acceptor based on the structure of the metabolic cofactor coenzyme Q<sub>10</sub>, which has previously been shown to exhibit redox-switchable quenching of luminescence of CdSe/ZnS core/shell QDs, although high populations of quinones were required to achieve acceptable levels of quenching efficiency.<sup>7</sup> In contrast, the system described here is designed to exploit the charge-separating properties of the type-II heterostructure of CdTe/CdS QDs, and is shown to possess a particularly efficient and switchable charge transfer-mediated quenching of luminescence that occurs via a high-lying surface electron trap state. In this study, steady state optical spectroscopy in combination with photoluminescence (PL) lifetime and ultrafast transient absorption spectroscopy are used to investigate the excited state dynamics of these conjugates and demonstrate their viability as high-sensitivity fluorimetric redox sensors.

## 2. Methods

### 2.1 Steady state optical spectroscopy

Steady state photoluminescence spectra were obtained for 4 ml QD dispersions in MilliQ water using an Edinburgh Instruments FLS 980 spectrometer, with temperature maintained at 22 °C. All samples were magnetically stirred during data acquisition. Photoluminescent quantum yield (PLQY) measurements were made using the same spectrometer fitted with an integrating sphere, with excitation at 420 nm. UV-Visible absorption spectra were obtained of the same samples using an Agilent Cary 5000 series spectrophotometer with temperature maintained at 22 °C.

### 2.2 Sample Preparation

Samples with varying Q2NS:QD ratios were prepared in cuvettes in an oxygen-free environment via ligand exchange as described in supporting information, and diluted as required in degassed ultra-pure water. "Reduced" samples were prepared under oxygen-free conditions by adding a volume of an aqueous solution of 10% w/v sodium dithionite and 10% w/v sodium ascorbate equal to 5% of the sample volume and stirred within a cuvette. The samples were sealed under a protective atmosphere for analysis to reduce the effects of photooxidation.

### 2.3 Transient photoluminescence measurements.

A time correlated single photon counting (TCSPC) system (previously reported by Espinobarro-Velazquez et al<sup>21</sup>) was used to investigate the Photoluminescence (PL) decay transients. First, a mode-locked Ti:sapphire laser (Mai-Tai HP, spectra physics) is used to produce 100 fs pulses at a repetition rate of 80 MHz and 840 nm wavelength. The repetition rate is then reduced to 4 MHz by an acousto-optic pulse picker (APE select) and the initial wavelength halved (to 420 nm) via second harmonic generation (APE harmonic generator). These pulses were used to excite the samples with an average power of ~2 mW. The PL emission of the samples was collected and focused into a monochromator (Spex 1870c) and detected at the PL peak (560 nm) by a multi-channel plate (Hamamatsu R3809U-50). The time correlation of the detected photons was performed with the use of a PC electronics card (TCC900) from Edinburgh Instruments.

## 2.4 Transient absorption measurements.

For the transient absorption (TA) experiments, a Ti:sapphire amplifier system (Spectra Physics Solstice Ace) was used to generate 800 nm pulses at 1 kHz, as previously reported.<sup>22</sup> A portion of this beam was used to pump an OPA (Topas Prime) with an associated NIR-UV-Vis unit to achieve the pump pulses at 420, 450 and 480 nm (~10 nm full width at half-maximum, 100 fs, 250 nJ). The rest of the OPA output was passed through a sapphire crystal to generate a white light continuum which was used as the probe to record changes in absorption between 435 and 720 nm. Ultrafast broadband transient absorption measurements were carried out at randomly ordered time points in a Helios (Ultrafast Systems LLC) spectrometer (-20 ps to 3 ns, ~0.2 ps resolution). The samples were magnetically stirred to avoid photocharging effects during the measurements and low pump fluences were used to rule out the probability of absorbing more than one photon per pulse.<sup>23</sup>

## 2.5 Theoretical calculation of trap-Q2NS transfer rates

Surface trap-to-Q2NS transfer times were calculated, within the framework of the atomistic semiempirical pseudopotential model, as described by Zhu et al,<sup>16</sup> with the modification that here the acceptor state is separated from the QD surface by a "linker" approximated by a one-atom thick insulating arm. The length of the linker was calculated at  $704 \pm 6$  pm by simulating Q2NS within the software package pymol and measuring the distance from a sulfur atom to the centre of the nearest quinone ring after finding the minimum energy conformation.<sup>24</sup> The LUMO of Q2NS bound to the QDs was calculated from cyclic voltammetry data, which is available in the supporting information.

# 3. Results & Discussion

## 3.1 Steady state luminescence spectroscopy

We synthesized QD-Q2NS conjugates with quinone:QD ratios of 40:1, 20:1 and 10:1, as well as a control sample with no Q2NS (referred to as 40Q, 20Q, 10Q, and 0Q, respectively). Details of procedure for synthesis of QDs and Q2NS as well as assembly of complexes are available in the supporting information. As each Q2NS molecule contains two quinone moieties, the notation used here refers to the number of quinones per QD, not the number of molecules of Q2NS per particle. Under ambient conditions, the quinones of Q2NS will be in the oxidized state and thus will be electron acceptors. Figure 1 compares the PL spectra obtained for each of these samples, under both oxidising and reducing conditions. For samples 10Q, 20Q, and 40Q the luminescence was quenched by approximately 98.7%, 99.8%, and 99.9%, respectively, as measured by comparison of photoluminescent quantum yield (PLQY). The large decrease in PLQY was accompanied by a small blue shift (6 nm) in the luminescence peak position. This behaviour is consistent with a highly-efficient electron transfer event to the quinone. The blue shift is attributed to the slight size polydispersity of the QD sample; larger QDs which exhibit longer-wavelength emission are likely to possess more Q2NS due to increased surface area. The high degree of quenching contrasts to that achieved with CdSe/ZnS core/shell QDs where a maximum quenching efficiency of 77% was observed with a far higher ratio of quenchers to QDs (~100).<sup>7</sup> The addition of chemical reducing agents (sodium dithionite and sodium ascorbate) suppressed the quenching effects of the Q2NS to an extent proportional to the number of quinones per QD, consistent with almost total suppression of the electron transfer process that causes quenching. The fact that PL does not recover to 100% of that exhibited by the control QDs is attributed to incomplete reduction of quinones in the aqueous environment, which cannot be made totally free of oxidants such as diatomic oxygen. For the 0Q sample, the PL was red-shifted with respect to that of the 10Q, 20Q, and 40Q samples after addition of the reducing agents. This is attributed to passivation

of surface traps by the Q2NS, which employs a thiolate binding complex.<sup>25</sup> The general increase in PL intensity after introduction of the reducing agent for 0Q is separately attributed to environmental passivation of trap states by the reducing agent mixture, which is corroborated by transient PL and transient absorption data.

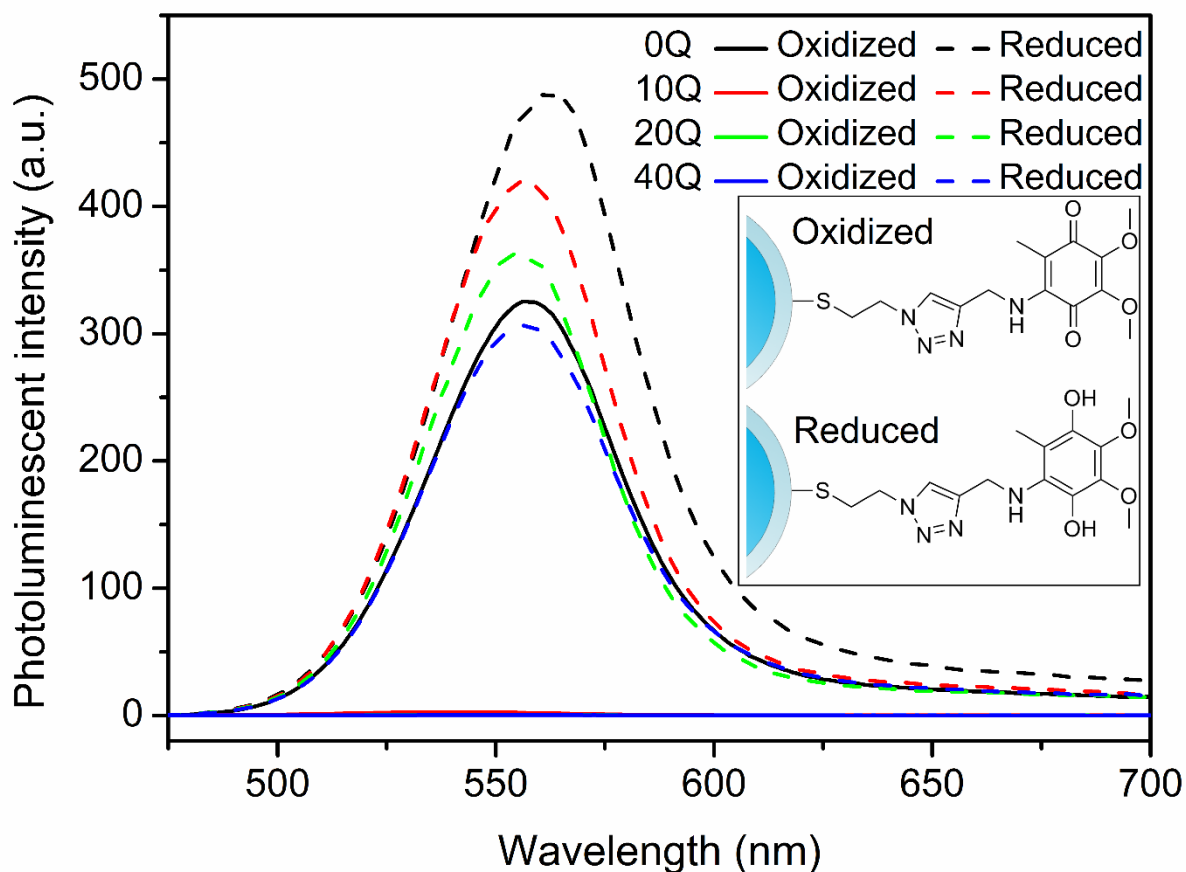


Figure 1. Photoluminescence spectra (for excitation at 420 nm) of QD samples (0Q, 10Q, 20Q and 40Q, in black, red, green and blue respectively) before (solid) and after (dashed) chemical reduction of surface bound Q2NS. Aside from control (0Q), oxidized samples are significantly (>98%) quenched compared to reduced samples, which exhibit strong luminescence at  $556 \pm 1$  nm. The inset shows the molecular structure of QD-bound Q2NS in oxidized (top) and reduced (bottom) states.

### 3.2 Measurement of per-quinone quenching efficiency

A consequence of the presence of a “linker” between the QD and quinone acceptor group is that each acceptor is likely only to be responsible for the quenching of luminescence of a single QD. Importantly for small acceptor:QD ratios, the population of Q2NS bound to the QDs can be assumed to follow Poissonian statistics.<sup>15</sup> For a given Q2NS:QD ratio  $\lambda$ , the luminescence quantum yield (PLQY) can therefore be expressed as

$$I_{\lambda} = I_0 \sum_{n=0}^{\infty} \frac{\lambda^n e^{-\lambda}}{n!} (1 - 2\kappa_q)^n \quad (1)$$

where  $\kappa_q$  is the per-quinone quenching efficiency, defined as the probability that a single quinone group will quench an event that would otherwise result in radiative recombination, with  $\kappa_{\text{mol}} = 2\kappa_q$  as the per-molecule efficiency. The parameter  $\kappa_q$  is related to the Stern-Volmer quencher rate coefficient

$k_q$  by the expression  $\kappa_q = k_q\tau$ , where  $\tau$  is the excitation lifetime. In equation 1, the parameter  $n$  is the number of Q2NS on any particular QD, found with probability  $P(n) = \frac{\lambda^n e^{-\lambda}}{n!}$ , and  $I_0$  is the PLQY for an unquenched sample.

To measure the efficiency  $\kappa_q$ , Q2NS:QD conjugates were prepared with Q2NS:QD ratios of 0 to 10. Figure 2 shows the measured PLQY for these samples; the above expression was fitted using a weighted least-squares regression scheme to his data, as also shown in Figure 2, resulting in a value for  $\kappa_q = 0.21 \pm 0.02$ . The close fit of the experimental data to the model described above agrees with the notion that Q2NS is permanently bound to the QDs, and importantly that each quinone is responsible for the quenching of PL of only one QD.

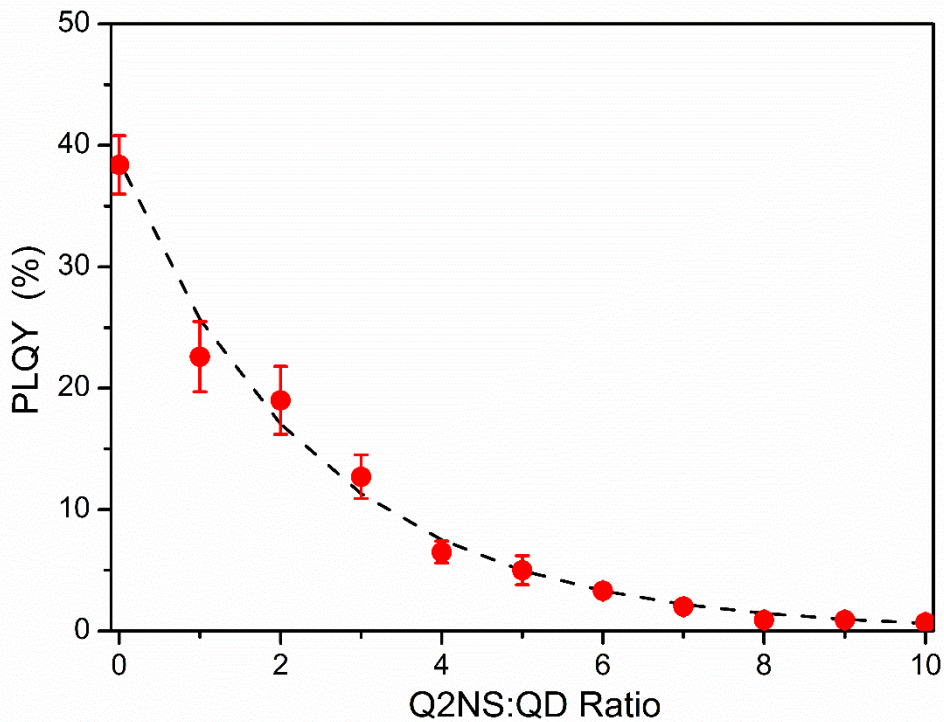


Figure 2. Photoluminescent quantum yield (PLQY) vs Q2NS:QD ratio for CdTe/CdS core/shell QDs conjugated to Q2NS (red circles). The dashed line represents a weighted least-squares fit to a statistically-derived function (eq. 1) which gives the per-quinone quenching efficiency as  $\kappa_q = 0.21 \pm 0.02$ .

### 3.3 PL Lifetime

Figure 3 shows the transient PL decays of samples 0Q, 10Q, 20Q and 40Q, with the corresponding bi-exponential or tri-exponential fits, both in the oxidized and reduced state. For the oxidized state data, two very distinctive behaviours can be observed for samples with and without Q2NS. Samples 10Q, 20Q and 40Q display a significant and rapid drop in PL intensity, which requires a tri-exponential fit to be adequately described, and is characterised by time constants of  $\tau_1^{PL} = 140 \pm 10$  ps,  $\tau_2^{PL} = 460 \pm 30$  ps and  $\tau_3^{PL} = 4000 \pm 900$  ps. Note that the response time of this experiment is  $100 \pm 10$  ps (see SI) i.e. similar to  $\tau_1^{PL}$ , and so the underlying process, or processes, associated with this decay constant are not resolved and hence may be significantly faster than the value of  $\tau_1^{PL}$ . On the other hand, the sample 0Q shows a much slower decay that can be fitted by a bi-exponential equation using only  $\tau_2^{PL}$  and  $\tau_3^{PL}$ . This is a clear indication that a fast charge transfer occurs from the QDs to the oxidized Q2NS, causing the quenching observed in static PL measurements. In contrast, only small

differences are observed between the samples with and without Q2NS in the reduced state. Samples with reduced Q2NS (10Q, 20Q and 40Q) no longer show the abrupt decay observed when they were in oxidized state and are only slightly faster as the quinone concentration increases. The small discrepancies between transient PL traces of reduced samples agree with the recovery in PL shown in figure 1, and are again attributed to incomplete reduction of quinones. The fastest time constant ( $\tau_1^{PL}$ ) is no longer needed to fit these decays, which can be now regarded as bi-exponential. The absence of this fast decay component agrees with the recovery in PL intensity observed for samples after reduction, and demonstrates that reduced quinone molecules no longer act as electron acceptors. Moreover, the difference between both decays for the sample 0Q in oxidized and reduced state suggest that in addition to reducing the quinone molecules, the reducing agent may also be inhibiting other non-radiative relaxation paths, e.g. passivating surface states. Further details on the decay fitting and analysis of the resulting parameters are given in the supporting information.

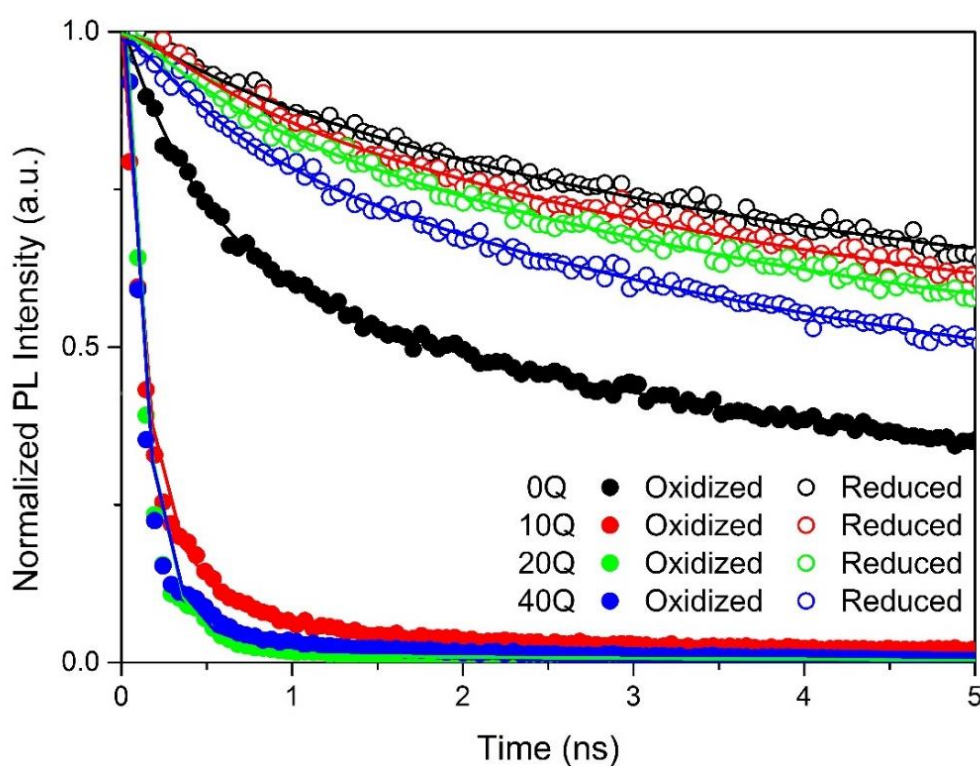


Figure 3. PL decay traces of samples in oxidized (filled circles) and reduced state (empty circles) for samples 0Q (black), 10Q (red), 20Q (green) and 40Q (blue). Bi-exponential or tri-exponential fits are displayed as continuous lines.

### 3.4 Transient Absorption Spectroscopy

The insets in figure 4 show, for a pump photon energy of 2.95 eV (i.e. a pump wavelength of 420 nm), the pump-induced absorbance change,  $\Delta A$ , spectra for each of the samples in both the oxidized and reduced states. Each spectrum exhibits a prominent bleach that corresponds to the peak in the steady-state absorbance spectra (see supporting information, figure S2). Also shown in Figure 4 are the first 50 ps of the corresponding fractional absorbance change,  $\Delta A/A$ , transients obtained at the peak of these bleach features with a tri-exponential fit to each of the decays; the full transients

are given in the SI. It has been established previously that this bleach is due to state-filling by electrons at the conduction band minimum (CBM), and the value of  $\Delta A/A$  is determined by the average occupation of the CBM<sup>26</sup>. These bleach transients rapidly reach an initial peak that then decays to a plateau over a few 10s of ps. This is typically observed in colloidal QD systems in which hot electrons created by the high energy pump pulse quickly cool down to the CBM giving rise to the initial peak. The decay is then produced by sub-nanosecond depopulation of the CBM, including by trapping of these cooled electrons, while the plateau represents long-lived electrons that may eventually contribute to emission by radiative recombination. It has been shown previously that samples of CdTe QDs are typically not homogenous<sup>27, 28</sup> but rather contain some subset of the population that is trap-free. The presence of a significant TA plateau confirms the presence of such a trap-free subset, or at least one with a much reduced trapping rate, and explains how a PLQY of near 40% can be observed when the trapping rate found from the TA decay greatly exceeds the rate of radiative recombination. (Sub-nanoseconds decays to a plateau can also occur in principle due to the Auger recombination of multi-excitons produced by the absorption of more than one photon per QD per excitation pulse.<sup>29</sup> However, the excitation fluences used in this study were always sufficiently low to make the probability of this process negligible – see SI for more detail<sup>23, 30</sup>) For the case of samples in an oxidized state, a significant decrease in the peak amplitude can be seen for the samples with Q2NS in comparison to the sample without, and the peak amplitude decreases more as the proportion of Q2NS increases (reaching only approximately 40 %, 30 % and 25 % of the peak 0Q amplitude for 10Q, 20Q and 40Q, respectively). This suggests that a substantial fraction of the hot electrons are extracted from the QD by the quinones of Q2NS before they can cool to the CBM. Furthermore, the amplitudes at the plateau have been reduced almost to zero for the samples with Q2NS, consistent with the observed PL quenching. This indicates that the electrons that do cool to the CBM can also be transferred to the oxidized quinones. After the samples have been reduced, a large increase in both peak and plateau amplitudes is observed for samples with Q2NS; in contrast, for the 0Q sample only a slightly larger bleach signal is seen. The fact that the 0Q sample shows improved PL intensity, longer PL decays and larger bleach signals after being exposed to the reducing agent implies that besides changing the oxidation state of the quinones, the reduction process also affects other non-radiative relaxation paths. The decay transients for all samples are well described by a tri-exponential fit with time constants of  $\tau_1^{TA} = 2.0 \pm 0.1$  ps,  $\tau_2^{TA} = 13.4 \pm 0.8$  ps and  $\tau_3^{TA} = 475 \pm 45$  ps. The longest of these time constants,  $\tau_3^{TA}$ , agrees well with the value of  $\tau_2^{PL}$  whilst the other two,  $\tau_1^{TA}$  and  $\tau_2^{TA}$ , are much shorter than the time response of the PL lifetime experiment and so would not be resolved by it, but would both still contribute to the amplitude associated with  $\tau_1^{PL}$ . The amplitudes associated with each of these components, in both the oxidized and reduced states, are given in the Supplementary Information for each sample. These data show that increasing the ratio of oxidized quinones to the QDs enhances the amplitude associated with the  $\tau_1^{TA}$  at the expense of those associated with  $\tau_2^{TA}$  and  $\tau_3^{TA}$ , indicating that it is  $\tau_1^{TA}$  that is associated with the electron transfer process from QD to oxidized Q2NS. Overall, the decay parameters for both transient PL and TA measurements are broadly similar to those observed for other colloidal QD systems, including CdTe/CdS QDs.<sup>20, 27, 31</sup>

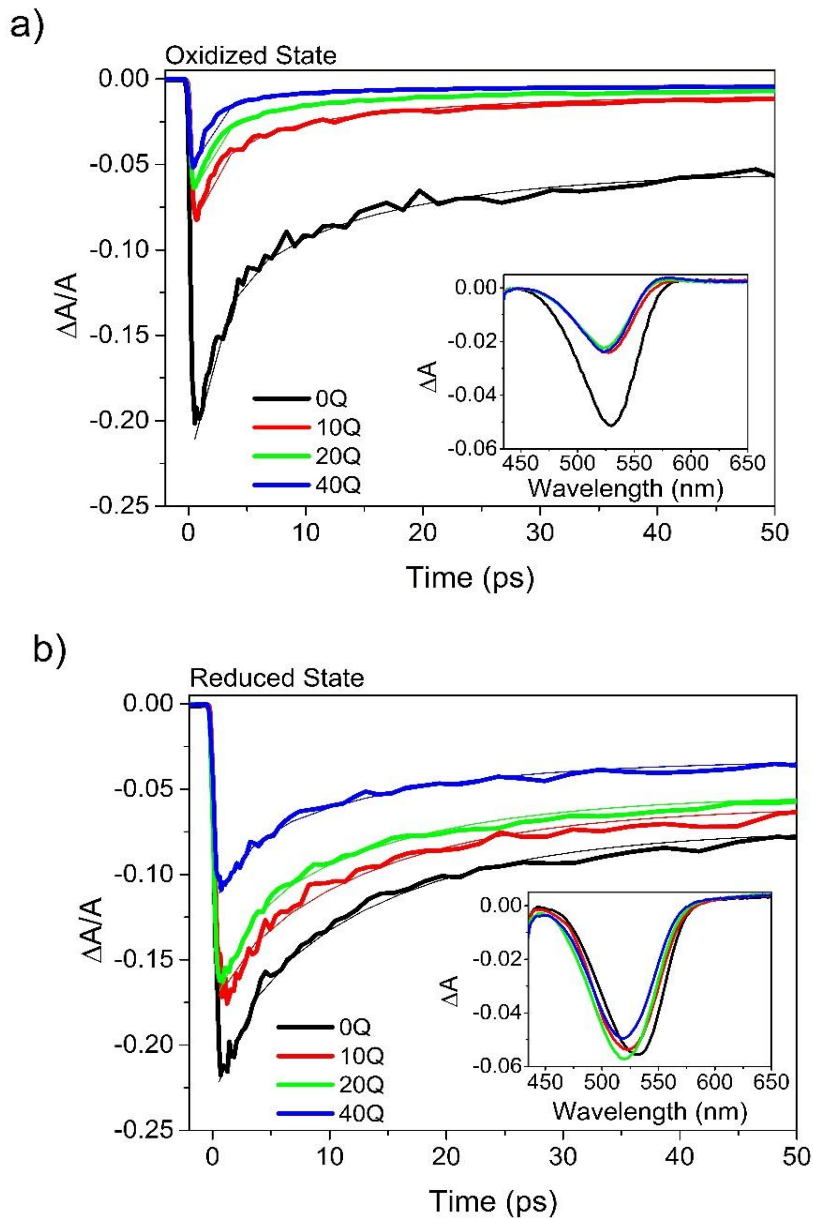


Figure 4. Fractional changes in absorption for samples in a) oxidized and b) reduced states following excitation at 420 nm with a fluence of  $2.5 \times 10^{-6} \text{ J cm}^{-2}$  and detected at the band edge (530 nm) with the corresponding tri-exponential fits. Insets are the corresponding absorbance change spectra obtained at a time corresponding to the peak amplitude.

To study the energy dependence of the initial electron transfer process, absorption transients were also obtained for pump photon energies of 2.75 eV and 2.58 eV, corresponding to pump wavelengths of 450 nm and 480 nm, respectively. Figure 5 shows for samples 0Q and 40Q, in both the oxidized and reduced state, the bleach transients obtained for all the three pump wavelengths; in each case, the bleach amplitude has been normalised by absorbed photon flux density at the different pump wavelengths. The peak bleach obtained is about 6-fold less for the oxidized 40Q sample compared to the oxidized 0Q samples at all pump wavelengths, indicating that transfer to Q2NS is competitive with hot electron cooling for all these initial excitation energies and so reduces the

number of electrons reaching the band edge. However, for both the oxidized 40Q and 0Q samples the peak bleach for pumping at 420 nm is about one-third of that obtained when pumping at either of the other two wavelengths, showing that there is a significant additional trapping of hot electrons excited to a higher energy level by this pump wavelength. After reduction, the transients for the both the 40Q and 0Q samples are broadly similar to the transients for the oxidized 0Q samples, showing that the electron transfer to the Q2NS has largely been switched off. However, the initial amplitudes of the reduced samples when pumped at either 450 nm or 480 nm were reduced compared to the oxidized 0Q, by a third and half for the reduced 0Q and 40Q, respectively. This is attributed to the effect of the reducing agents on the hot trapping process, which has been shown previously to be sensitive to surface treatments,<sup>27, 32</sup> and also indicates that there is some hot trapping occurring for pumping at 450 nm and 480nm, as well as at 420 nm.

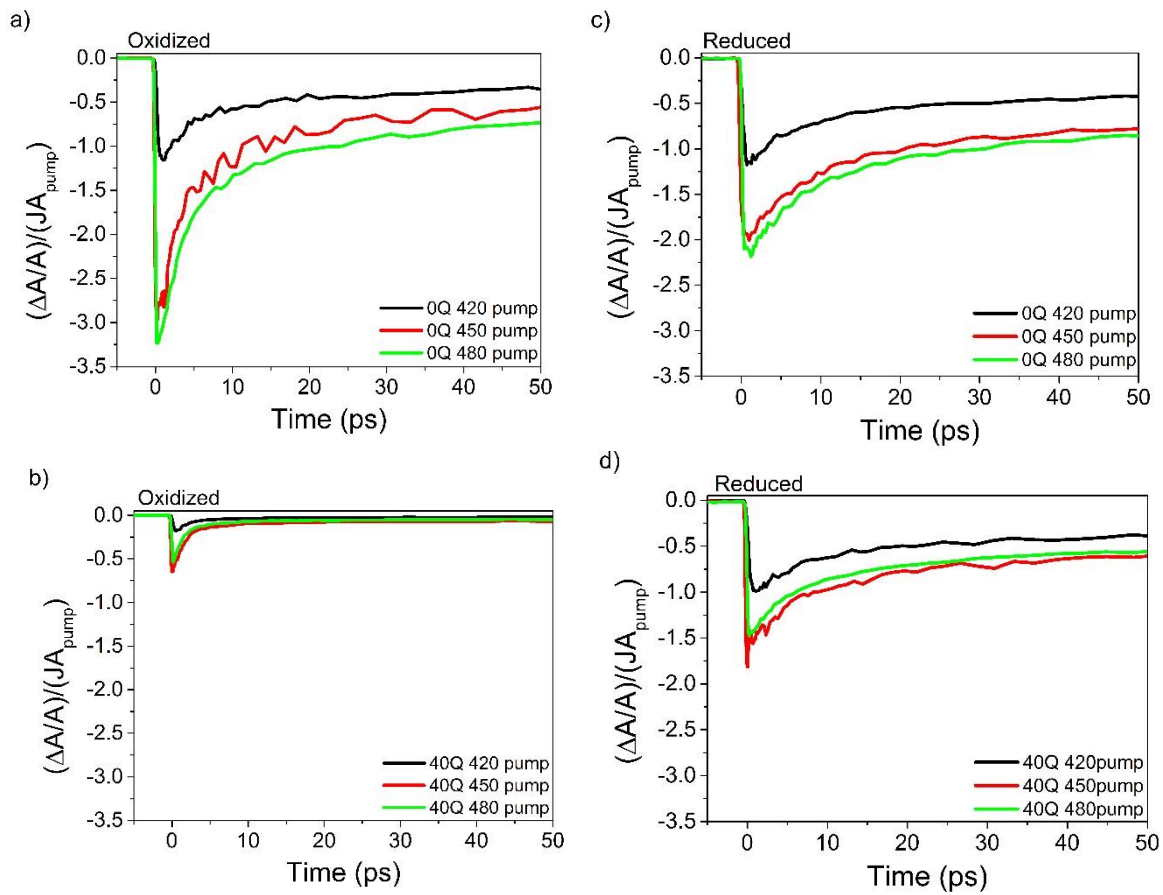


Figure 5. Fractional changes in absorption for samples a) 0Q in oxidized state, b) 40Q in oxidized state, c) 0Q in reduced state and d) 40Q in reduced state obtained at an absorbed photon flux density,  $JA_{\text{pump}}$ , of  $1.7 \times 10^{12}$  photons  $\text{cm}^2$  per pulse.

### 3.5 Modelling Transfer rates

To gain further insight into the nature of the electron transfer process, calculations for transfer times for a simplified CdTe core QD-acceptor system were performed within the framework of the atomistic semiempirical pseudopotential method.<sup>33</sup> The QD core is represented by a CdTe core particle of radius 3 nm. To ensure the absence of any electronic coupling between QD and acceptor, the "linker" part of

Q2NS was modelled as a one-atom-thick arm made of a zinc blende semiconducting material with a band gap much greater than that of CdTe. The Q2NS was modelled, according to an established procedure,<sup>16</sup> as a localised acceptor state positioned at the end of the linker, whose energy coincided with our experimental estimate for the lowest unoccupied molecular orbital (LUMO) of Q2NS. For direct transfer of an electron from the CBM, calculated transfer times are of the order of nanoseconds, and increase for electrons excited to higher energy states. These transfer times are significantly longer than what is observed from TA measurements. Transfer times from a simulated surface trap state, however, agree closely with those observed. Depending on the relative position of the simulated trap state and attached acceptor, predicted transfer times range from a few (2-8) ps for the shortest distance trap, to tens (40-70) of ns for the furthest, covering all values in between. The transfer times are calculated assuming an Auger-mediated process,<sup>16</sup> whose rates depend on the dielectric constant of the nanocrystal's environment.<sup>34</sup> We considered dielectric constants varying from 2.5 to 6 in order to represent the effects of ligands, solvents and shell material. The variation in the calculated transfer times for each particular distance accounts for this variation in dielectric environment. These simulations strongly suggest transfer to the Q2NS is dominated by a stepwise process involving an intermediate surface trap state. Despite the simplicity of this approach, where the linker is replaced by an atomic chain made of an insulating material and the electron acceptor is modelled only through the position of its LUMO, our calculated transfer rates reproduce well the observed trends, particularly when considering the large number of quinones per QD.

These observations and calculations are thus consistent with a step-wise electron transfer process: hot electrons can be trapped in a localised QD state, at an energy that lies above the CBM, rather than cool directly to the band edge regardless of the presence of Q2NS, whether oxidized or reduced; such trapped electrons can (i) cool to the band edge, (ii) non-radiatively recombine or (iii) transfer to an oxidized quinone (if present), with the latter able to largely outcompete the others. Electrons that have reached the CBM can also transfer to an oxidized quinone or can recombine, either radiatively or non-radiatively. A schematic diagram showing the energy levels in the QD and the possible charge excitation and relaxation processes is given in figure 6.

It has been previously reported that for similar CdTe/CdS core shell QDs, the absorption transition occurs between states associated with the core only, and the resulting excited electron is localised to the CdS surface.<sup>19, 20</sup> This serves to increase the recombination lifetime, and further suggests that the trap state associated with efficient transfer is a surface electron trap state associated with under-coordinated cations.<sup>35, 36</sup>

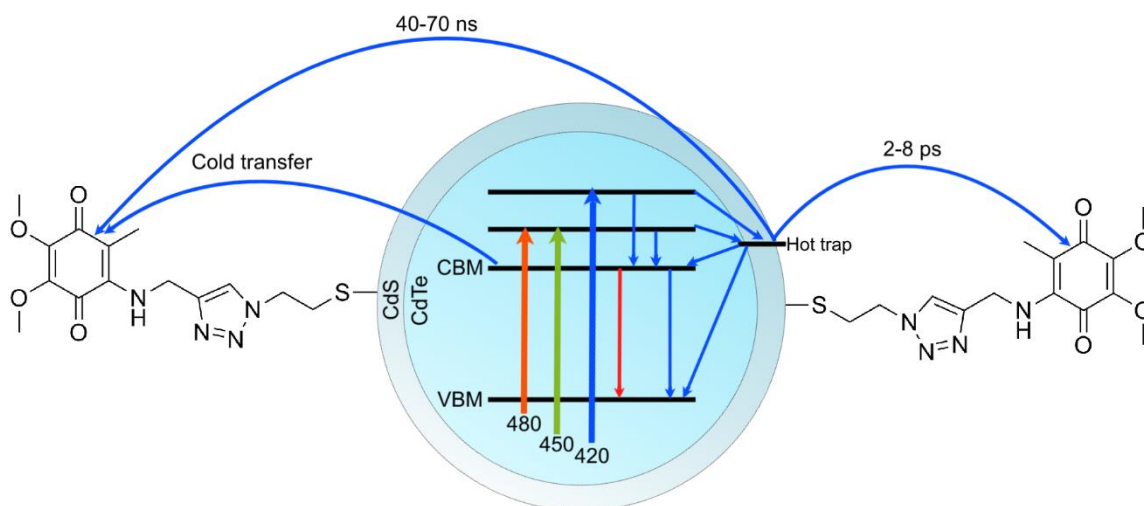


Figure 6. Schematic diagram of quantum dot energy levels and possible charge excitation and relaxation processes for CdTe/CdS core/shell QDs conjugated to Q2NS. Thick colored lines represent excitation at 480 nm (orange) 450 nm (green) and 420 nm (blue). Thin blue lines represent non-radiative processes, and the thin red line represents radiative recombination. Pumping at 2.95 eV (420 nm) allows efficient electron transfer to attached Q2NS via a high-lying intermediate surface trap state. The efficiency of this transfer is strongly dependent on the spatial separation of the attached Q2NS acceptor and trap state donor.

#### 4. Conclusion

We have optimised the design of redox-sensitive QD-acceptor conjugates by employing a switchable ultrafast trapping scheme. Transient absorption spectroscopic data, combined with analysis of PL lifetime data showed that electron transfer from colloidal CdTe/CdS QD to a surface bound electron acceptor is possible both by “hot” electrons and those that have cooled to the CBM. Analysis of the absorption bleach at varying wavelengths implicates a particular hot trap state that exhibits efficient transfer to the Q2NS. Transfer timescales predicted by calculations within the framework of the semiempirical atomistic pseudopotential method concur with these experimental observations. Upon chemical reduction of Q2NS, electron transfer from the QD is seen to be suppressed, so electrons cool to the band edge and undergo recombination as normal. Employing this bimodal electron transfer route greatly increases the quenching efficiency of the QD-acceptor system vs other QDs, and extends their applicability as a useful biosensor. In addition to this, the new insight that hot trapped electrons can be efficiently extracted from the QDs using this organic molecule may have important consequences for device design.

#### 5. Acknowledgements

A Harvie thanks the University of Leeds and AstraZeneca for contributions to funding. C Smith thanks the EPSRC (EP/K008544/1) for financial support. R Ahumada-Lazo thanks CONACYT for provision of a scholarship (284566/399936). L Jeuken thanks the BBSRC (BB/K009753/1) for financial support. K Critchley thanks the EPSRC (EP/P005233/1) and MRC (MR/K015613/1) for financial support. Transient absorption measurements were performed at the Ultrafast Biophysics Facility, Manchester Institute of Biotechnology, as funded by BBSRC Alert14 Award BB/M011658/1.

Supporting information available: The information includes detailed procedures for synthesis of the QD-acceptor conjugates, particle sizing, cyclic voltammetry, and further information on the analysis of TA and PL lifetime data. This information is available free of charge via the Internet at <http://pubs.acs.org>.

## 6. References

1. Michler, P.; Kiraz, A.; Becher, C.; Schoenfeld, W. V.; Petroff, P. M.; Zhang, L.; Hu, E.; Imamoglu, A. A Quantum Dot Single-Photon Turnstile Device. *Science* **2000**, *290* 2282-2285.
2. Kamat, P. V. Quantum Dot Solar Cells. The Next Big Thing in Photovoltaics. . *J. Phys. Chem. Lett.* **2013**, *4*, 908-918.
3. Wood, V.; Bulovic, V. Colloidal Quantum Dot Light-Emitting Devices. *Nano Rev.* **2010**, *1*.
4. Medintz, I. L.; Uyeda, H. T.; Goldman, E. R.; Mattoussi, H. Quantum Dot Bioconjugates For Imaging, Labelling And Sensing. *Nat. Mater.* **2005**, *4*, 435-446.
5. Algar, W. R.; Tavares, A. J.; Krull, U. J. Beyond labels: A Review Of The Application Of Quantum Dots As Integrated Components Of Assays, Bioprobes, And Biosensors Utilizing Optical Transduction. *Anal. Chim. Acta.* **2010**, *673*, 1-25.
6. Auchinvole, C. A. R.; Richardson, P.; McGuinness, C.; Mallikarjun, V.; Donaldson, K.; McNab, H.; Campbell, C. J. Monitoring Intracellular Redox Potential Changes Using SERS Nanosensors. *ACS Nano* **2012**, *6*, 888-896.
7. Ma, W.; Qin, L.-X.; Liu, F.-T.; Gu, Z.; Wang, J.; Pan, Z. G.; James, T. D.; Long, Y.-T. Ubiquinone-Quantum Dot Bioconjugates For In Vitro And Intracellular Complex I Sensing. *Sci. Rep.* **2013**, *3*, 1537.
8. Heiden, M. G. V.; Cantley, L. C.; Thompson, C. B. Understanding the Warburg Effect: The Metabolic Requirements of Cell Proliferation. *Science* **2009**, *324*, 1029-1033.
9. Jorgenson, T. C.; Zhong, W.; Oberley, T. D. Redox Imbalance and Biochemical Changes in Cancer. *Cancer Res.* **2013**, *73*, 6118-6123.
10. Nielsen, J. L.; Aquino de Muro, M.; Nielsen, P. H. Evaluation Of The Redox Dye 5-Cyano-2,3-Tolyl-Tetrazolium Chloride For Activity Studies By Simultaneous Use of Microautoradiography and Fluorescence In Situ Hybridization. *Appl. Environ. Microbiol.* **2003**, *69*, 641-643.
11. Medintz, I. L.; Stewart, M. H.; Trammell, S. A.; Susumu, K.; Delehanty, J. B.; Mei, B. C.; Melinger, J. S.; Blanco-Canosa, J. B.; Dawson, P. E.; Mattoussi, H. Quantum-Dot/Dopamine Bioconjugates Function as Redox Coupled Assemblies for In-vitro and Intracellular pH Sensing. *Nat. Mat.* **2010**, *9*, 676-684.
12. Freeman, R.; Willner, I. NAD<sup>+</sup>/NADH-Sensitive Quantum Dots: Applications to Probe NAD<sup>+</sup>-Dependent Enzymes and to Sense the RDX Explosive. *Nano Lett.* **2008**, *9*, 322-326.
13. Freeman, R.; Willner, I. Optical Molecular Sensing with Semiconductor Quantum dots (QDs). *Chem. Soc. Rev.* **2012**, *41*, 4067-4085.
14. Hildebrandt, N.; Spillmann, C. M.; Algar, W. R.; Pons, T.; Stewart, M. H.; Oh, E.; Susumu, K.; Diaz, S. A.; Delehanty, J. B.; Medintz, I. L. Energy Transfer with Semiconductor Quantum Dot Bioconjugates: A Versatile Platform for Biosensing, Energy Harvesting, and Other Developing Applications. *Chem. Rev.* **2016**, *117*, 536-711.
15. Peterson, M. D.; Cass, L. C.; Harris, R. D.; Edme, K.; Sung, K.; Weiss, E. A. The Role of Ligands in Determining the Exciton Relaxation Dynamics in Semiconductor Quantum Dots. *Annu. Rev. Phys. Chem.* **2014**, *65*, 317-339.
16. Zhu, H.; Yang, Y.; Hyeon-Deuk, K.; Califano, M.; Song, N.; Wang, Y.; Zhang, W.; Prezhd, O. V.; Lian, T. Auger-Assisted Electron Transfer from Photoexcited Semiconductor Quantum Dots. *Nano Lett.* **2014**, *14*, 1263-1269.
17. Rabouw, F. T.; de Mello Donega, C. Excited-State Dynamics in Colloidal Semiconductor Nanocrystals. *Top. Curr. Chem.* **2016**, *374*, 58.

18. Rawalekar, S.; Kaniyankandy, S.; Verma, S.; Ghosh, H. N. Surface-State-Mediated Charge-Transfer Dynamics in CdTe/CdSe Core-Shell Quantum Dots. *ChemPhysChem* **2011**, *12*, 1729-1735.
19. Rawalekar, S.; Kaniyankandy, S.; Verma, S.; Ghosh, H. N. Ultrafast Charge Carrier Relaxation and Charge Transfer Dynamics of CdTe/CdS Core-Shell Quantum Dots as Studied by Femtosecond Transient Absorption Spectroscopy. *J. Phys. Chem. C* **2009**, *114*, 1460-1466.
20. Wang, L.; Wang, H.-Y.; Gao, B.-R.; Pan, L.-Y.; Jiang, Y.; Chen, Q.-D.; Han, W.; Sun, H.-B. Transient Absorption Spectroscopic Study on Band-Structure-Type Change in CdTe/CdS Core-Shell Quantum Dots. *IEEE J. Quantum Electron* **2011**, *47*, 1177-1184.
21. Espinobarro-Velazquez, D.; Leontiadou, M. A.; Page, R. C.; Califano, M.; O'Brien, P.; Binks, D. J. Effect of Chloride Passivation on Recombination Dynamics in CdTe Colloidal Quantum Dots. *ChemPhysChem* **2015**, *16*, 1239-1244.
22. Brandariz-de-Pedro, G.; Heyes, D. J.; Hardman, S. J.; Shanmugam, M.; Jones, A. R.; Weber, S.; Nohr, D.; Scrutton, N. S.; Fielding, A. J. Direct Evidence of an Excited-State Triplet Species upon Photoactivation of the Chlorophyll Precursor Protochlorophyllide. *J. Phys. Chem. Lett.* **2017**, *8*, 1219-1223.
23. de Mello Donega, C.; Koole, R. Size Dependence of the Spontaneous Emission Rate and Absorption Cross Section of CdSe And CdTe Quantum Dots. *J. Phys. Chem. C* **2009**, *113*, 6511-6520.
24. O'Boyle, N. M.; Banck, M.; James, C. A.; Morley, C.; Vandermeersch, T.; Hutchison, G. R. Open Babel: an Open Chemical Toolbox. *Cheminform* **2011**, *3*, 33.
25. Borchert, H.; Talapin, D. V.; Gaponik, N.; McGinley, C.; Adam, S.; Lobo, A.; Moller, T.; Weller, H. Relations Between The Photoluminescence Efficiency of CdTe Nanocrystals and their Surface Properties Revealed by Synchrotron XPS. *J. Phys. Chem. B* **2003**, *107*, 9662-9668.
26. Klimov, V. I. *Nanocrystal Quantum Dots*. CRC Press: **2010**.
27. Smith, C. T.; Leontiadou, M. A.; Page, R.; O'Brien, P.; Binks, D. J. Ultrafast Charge Dynamics in Trap-Free and Surface-Trapping Colloidal Quantum Dots. *Adv. Sci.* **2015**, *2*.
28. Mahler, B.; Spinicelli, P.; Buil, S.; Quelin, X.; Hermier, J.-P.; Dubertret, B. Towards Non-Blinking Colloidal Quantum Dots. *Nat. Mat.* **2008**, *7*, 659.
29. Kobayashi, Y.; Pan, L.; Tamai, N. Effects of Size and Capping Reagents on Biexciton Auger Recombination Dynamics of CdTe Quantum Dots. *J. Phys. Chem. C* **2009**, *113*, 11783-11789.
30. Makarov, N. S.; Guo, S.; Isaienko, O.; Liu, W.; Robel, I.; Klimov, V. I. Spectral and Dynamical Properties of Single Excitons, Biexcitons, and Trions in Cesium-Lead-Halide Perovskite Quantum Dots. *Nano Lett.* **2016**, *16*, 2349-2362.
31. Wang, H.; de Mello Donega, C.; Meijerink, A.; Glasbeek, M. Ultrafast Exciton Dynamics in CdSe Quantum Dots Studied from Bleaching Recovery and Fluorescence Transients. *J. Phys. Chem B* **2006**, *110*, 733-737.
32. Page, R. C.; Espinobarro-Velazquez, D.; Leontiadou, M. A.; Smith, C.; Lewis, E. A.; Haigh, S. J.; Li, C.; Radtke, H.; Pengpad, A.; Bondino, F. Near-Unity Quantum Yields from Chloride Treated CdTe Colloidal Quantum Dots. *Small* **2015**, *11*, 1548-1554.
33. Wang, L. W.; Zunger, A. Pseudopotential Calculations of Nanoscale CdSe Quantum Dots. *Phys. Rev. B* **1996**, *53*, 9579-9582.
34. Califano, M.; Gómez-Campos, F. M. Universal Trapping Mechanism in Semiconductor Nanocrystals. *Nano Lett.* **2013**, *13*, 2047-2052.
35. Hines, M. A.; Guyot-Sionnest, P. Synthesis And Characterization of Strongly Luminescing ZnS-Capped CdSe Nanocrystals. *J. Phys. Chem.* **1996**, *100*, 468-471.
36. Kuno, M.; Lee, J.-K.; Dabbousi, B. O.; Mikulec, F. V.; Bawendi, M. G. The Band Edge Luminescence of Surface Modified CdSe Nanocrystallites: Probing the Luminescing State. *J. Chem. Phys* **1997**, *106*, 9869-9882.

## TOC Graphic

